Intensifying risk of mass human heat mortality if historical weather patterns recur

Christopher W. Callahan[1,*], Jared Trok[1], Andrew J. Wilson[2], Carlos F. Gould[3], Sam Heft-Neal[2], Noah S. Diffenbaugh[1], & Marshall Burke[1,2,4]

[1]Doerr School of Sustainability, Stanford University

[2]Center on Food Security and the Environment, Stanford University

[3]School of Public Health, University of California San Diego

[4]National Bureau of Economic Research

*Corresponding author: christophercallahan@stanford.edu

The potential death toll of worst-case extreme heat events is crucial for climate risk analysis and adaptation planning. We estimate this quantity for Europe using machine learning to calculate the intensity of historical heat waves if they occur at present or future global temperatures, combined with empirical exposure-response functions to quantify the resulting mortality. Each event is projected to generate tens of thousands of excess deaths. For example, if July 1994 or August 2003 meteorological conditions recur at the current global temperature anomaly of 1.5 °C, we project 14,000 or 17,300 excess deaths across Europe in a single week, respectively. At 3 °C, mortality rises to 26,800 or 31,500 per week. These death rates are comparable to peak COVID-19 mortality in Europe and are not substantially reduced by ongoing climate adaptation. Our results suggest that avoiding mass heat mortality in Europe will require significant and novel adaptation to heat.

Climate change is increasing the frequency and magnitude of extreme heat events (1–4), threatening human health (5). Additional warming is projected to generate more intense heat events than even recent record-breaking events (6), with the potential for mass mortality events similar to those witnessed in Europe in the summer of 2003 (7).

Projections of increased heat-related mortality from climate change are now numerous (8–13). However, these projections generally focus on the long-term population burden of non-optimal temperatures rather than the potential death toll of individual high-impact events. Exceptional extreme heat events require distinct management strategies compared to typical population burdens, straining triage and other resources not affected during milder temperatures (14). Preparedness for hospital overcrowding and health system surge capacity should therefore be benchmarked to a plausible worst-case scenario rather than the average of an aggregated projection (15).

Quantifying plausible worst-case scenarios under future climate change requires careful methodological treatment, and there are reasons to believe that existing projections do not capture the most extreme mortality events. The relatively short records of observations and global climate models (GCMs) make it difficult to assess the probabilities of the most extreme events (16), and GCMs poorly simulate the atmospheric circulation patterns that drive very extreme events (17). Progress has been made using tools such as initial-condition ensembles to quantify very rare heat mortality (18), but deficiencies remain in GCM simulations of atmospheric patterns governing heat extremes in populous regions such as Europe (19–22). Instead, a promising approach may be to develop "storylines" of heat waves that are physically plausible and dynamically consistent. This conditional approach, which emphasizes plausibility rather than probability (23), enables exploration of extreme outcomes (24) and stress tests of adaptation strategies (15, 25). Plausible storylines must also account for the documented ability of humans to adapt to repeated heat exposure, and to change behavior following past extreme heat episodes (26).

Major heat mortality events require multiple ingredients: large-scale physical drivers of elevated temperatures as well as human health responses to the resulting heat stress. Extreme heat events tend to occur when atmospheric high-pressure systems interact with dry soils to produce land-atmosphere feedbacks that amplify heat accumulation (6, 27–29).

In turn, when the human body is exposed to extended periods of high temperature, core temperature rises, cardiovascular activity is elevated, and illness and death can result (30).

Here, we focus on the combination of these geophysical and physiological ingredients in Europe. Hot extremes are increasing rapidly in Europe (31), with atmospheric circulation patterns contributing to warming that is faster than the rest of the hemisphere (19, 20, 27) and poorly simulated by GCMs (21, 22). Tens of thousands of deaths across the continent have been linked to recent summer heat (32, 33), with climate change contributing to more than half of these (34). As a result, Europe is a particularly timely setting in which to study the risk of mass heat mortality events.

We leverage two approaches to quantify the risk of mass heat mortality across Europe (Methods). First, we use a recently developed machine learning architecture (35) with two steps: convolutional neural networks are trained on an ensemble of GCMs to predict daily temperatures from the annual global mean temperature (GMT), calendar day, and modeled daily meteorological conditions; then, observed meteorological conditions are used as out-of-sample inputs to predict "counterfactual" versions of historical heatwave events at varying GMT. For this study, we produce counterfactual estimates of five multi-week periods of extreme heat that occurred in July 1994, August 2003, July 2006, June 2019, and August 2023. While these periods of extreme heat had differing durations and spatial extents, we choose them as illustrative events because each corresponds to a continuous period of Europe-wide temperature anomalies (specific date ranges shown in Fig. S1), shows spatial patterns of anomalous atmospheric pressure and soil moisture (Fig 1a, b), and spans a wide time period and range of human influence of climate system (e.g., annual GMT anomaly of 0.6 °C in 1994 vs. 1.5 °C in 2023).

Second, we use longitudinal data on temperature and weekly mortality over 2015-2019 from 924 subnational regions of Europe to estimate exposure-response functions that relate ambient temperature to mortality risk (Methods). We control for location-specific seasonal and trending factors, isolating plausibly exogenous variation in temperature to measure the causal effect of temperature on mortality. We then calculate mortality from each event at each GMT anomaly and compare it to a long-term average baseline without global warming.

These tools allow us to explicitly separate the effects of climate change and weather variability on heat-related mortality. We can leverage the diverse library of weather patterns simulated by GCMs to learn nonlinear relationships between meteorological patterns and surface heat extremes, along with the heterogeneity of responses to global warming across those specific patterns (35). At the same time, our out-of-sample application of these learned relationships to observed meteorological patterns grounds our analysis in weather systems that have historically produced extreme heat. Whereas previous studies of climate change and mortality in Europe have been limited to either linear scaling to capture multiple events (34) or computationally-intensive custom simulations for an individual event (36), our approach allows us to leverage a large ensemble of simulations to predict the temperature profiles that result from numerous different historical meteorological conditions at multiple global temperatures.

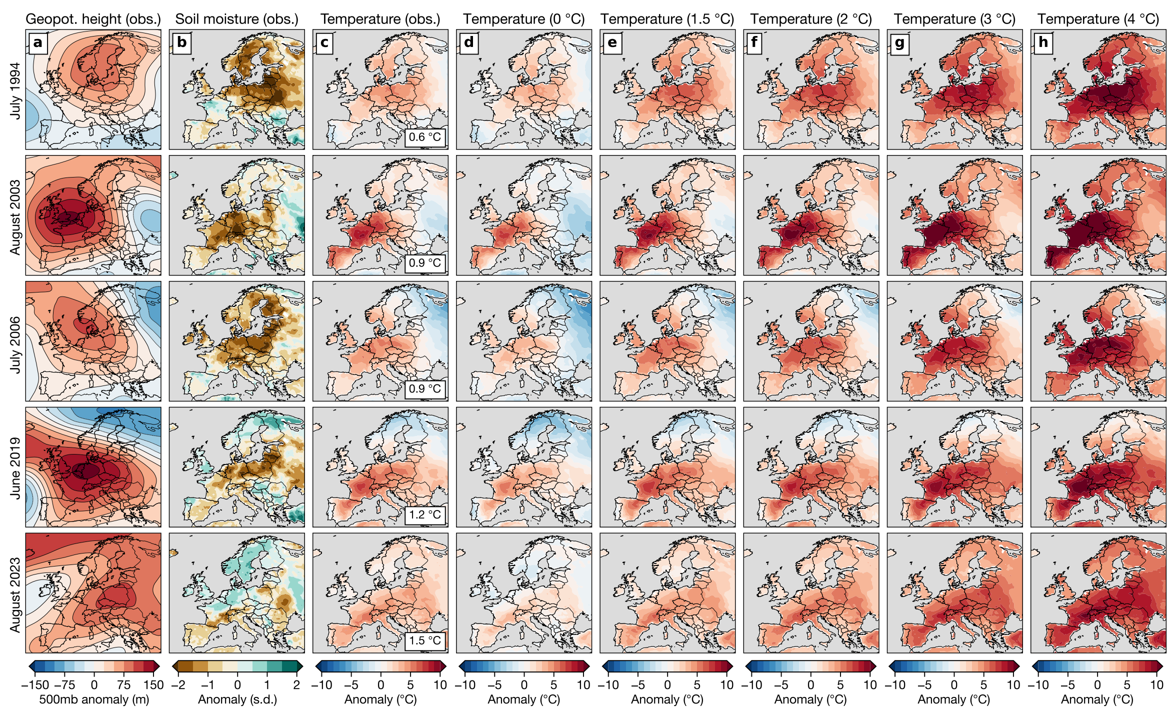

Figure 1: Observed and counterfactual heat waves in Europe. a-c) Observed 500-mb geopotential height (a), soil moisture (b), and temperature (c) anomalies during five selected extreme heat events (from top to bottom: July 1994, August 2003, July 2006, June 2019, and August 2023). Inset text in (c) denotes the GMT anomaly in the corresponding year. d-h) Counterfactual temperature anomalies during each of the five heat waves at GMT anomalies of 0 (d), 1.5 (e), 2 (f), 3 (g), and 4 (h) °C. All GMT anomalies are defined relative to 1850-1900. Meteorological anomalies are relative to the location and day-of-year mean over 1979-2023 and averaged over the days defined for each event (Fig. S1).

Results

While the precise meteorological conditions associated with each illustrative heat wave vary, they share common characteristics: anomalous high-pressure systems (Fig. 1a) and dry soils across much of the continental interior (Fig. 1b), resulting in elevated temperatures across many countries (Fig. 1c).

Without global warming, each of these events would have been cooler (Fig. 1d, Fig. S2), consistent with previous work (e.g., 37). Likewise, with additional global warming, the same meteorology for a given event would produce steadily more intense temperature anomalies (Fig. 1e-h, Fig. S2). The difference between the actual event magnitude and the magnitude at different annual GMT varies by event, both because the actual events occurred at different GMT and because the response to global warming varies between meteorological patterns (35). Across annual GMT of 1.5, 2, 3, and 4 °C, the August 2003 meteorological conditions yield the highest temperatures of all events, emphasizing the severity of the conditions during that event (38). Similarly, July 1994, for which observed temperature anomalies were relatively moderate among the illustrative events, produces among the most severe anomalies when predictions are made at standardized GMTs (Fig. 1).

High temperatures are empirically associated with increased mortality risk across Europe (Fig. 2). Consistent with previous work (9), we specifically find that the heat-mortality relationship is moderated by a region's long-term mean temperature; for example, the minimum mortality temperature (MMT) is 14.4 °C in the coolest third of regions and 19.7 °C in the warmest third of regions. This heterogeneity may reflect the greater return on adaptation investments such as air conditioning in warmer regions (9). However, the slope of the exposure-response curve is steeper for warmer areas despite their higher MMT, potentially reflecting limits to adaptation to the hottest conditions. For all regions, the nonlinear increase in mortality risk above the MMT means that greater extreme heat intensity is expected to increase mortality across the continent (Fig. 2, lower inset points).

Each extreme heat event is projected to generate thousands of weekly excess deaths across Europe at the current annual GMT of 1.5 °C (39), with increasing impacts in response to larger GMT anomalies (Fig. 3, Table S1). The largest death tolls are associated with the 1994 and 2003 conditions (Fig. 3a, b), with 26,865 and 31,620 weekly excess deaths in a 3 °C

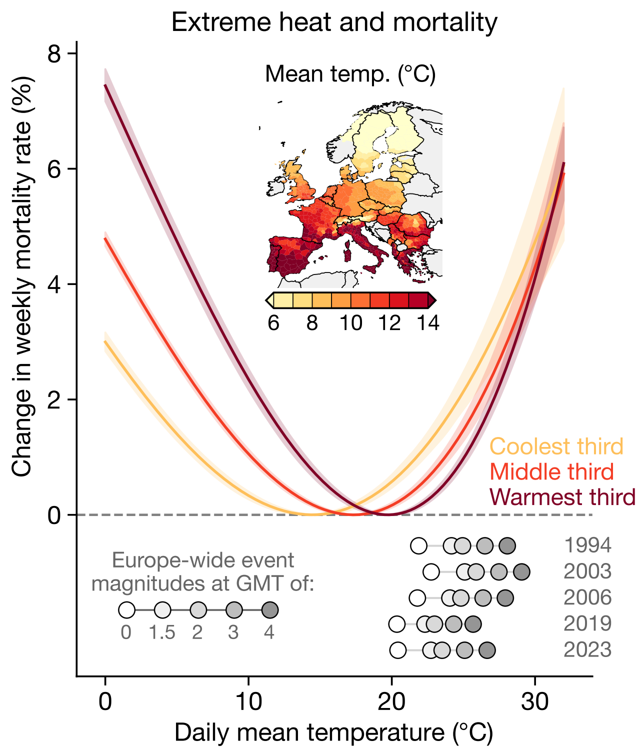

Figure 2: Temperature-mortality relationship across Europe. Relationship between daily temperatures and cumulative weekly mortality rate change in subnational regions across Europe as a function of regions' 2000-2019 mean temperature. Curves show examples for the coolest third (yellow), middle third (orange), and warmest third (red) of regions. Effects are accumulated across the contemporaneous week and the following three weeks by including three lags in the regression (Methods). Each curve is referenced to its own minimum mortality temperature. Map shows mean temperature for each region; only regions for which we have mortality data are colored. Lower inset points show the population-weighted Europe-wide average temperature during each event at a range of annual GMT anomalies.

year, respectively. While less likely than more moderate temperatures given current emissions trends, individual years at 4 °C are still plausible under gradual decarbonization (40), and would generate 39,295 (1994) and 45,266 (2003) excess deaths in a single week across Europe if these meteorological conditions recurred. The other three events are associated with weekly peaks of 24,721, 17,657, and 20,183 excess deaths, respectively, at 3 °C. Excess mortality is slightly negative in the weeks following the event, consistent with mortality displacement (Methods), though not enough to offset the peak of the event.

These death tolls reflect the underlying effect of hot temperatures without climate change, combined with the influence of climate change in intensifying these events. Comparing each event to a counterfactual event at 0 °C allows us to isolate the contribution of climate change to event mortality (red lines vs. gray shading in Fig. 3). For example, at the peak weekly mortality rate of a 2003-like event at 3 °C, we project climate change to produce an additional 23,154 excess deaths on top of 8,467 that would have occurred without warming, making anthropogenic warming responsible for 73% of the death toll (Table S2).

The spatial distribution of mortality during each event differs, governed by the location of temperature anomalies (Fig. 1), variation in exposure-response functions (Fig. 2), and

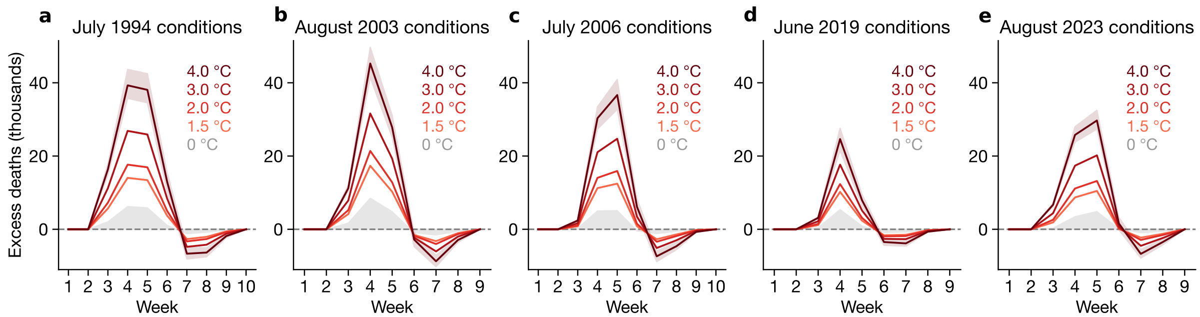

Figure 3: Mortality during counterfactual extreme heat events. Europe-wide weekly excess mortality during extreme heat events based on meteorological conditions from July 1994 (a), August 2003 (b), July 2006 (c), June 2019 (d), and August 2023 (e) across a range of annual global temperatures. Solid line shows average projection and shading shows 95% range. Gray shading shows mortality at 0 °C, meaning the mortality that would have occurred without global warming; the contribution of warming is the difference between each colored line and the gray shading. The x-axis spans two weeks before the event begins to three weeks after it ends to illustrate the lagged effects of the event on mortality (Methods).

spatial variation in the effect of global warming (Fig. S3). For example, under 1994-like conditions, the greatest mortality occurs in Germany, Poland, and Eastern Europe, whereas under 2023-like conditions, mortality is highest in Spain, Italy, and the Balkans (Fig. S4).

Given that European countries undertook adaptation to heat following previous events such as 2003 (26), and we observe heterogeneity in exposure-response functions that may indicate adaptation (Fig. 2), we explore the potential for additional future adaptation to mitigate mortality from these events. (Our exposure-response functions are trained over 2015-2019, meaning they likely already incorporate any adaptation that occurred after 2003.) Specifically, we allow each region's mean temperature to evolve in the future according to pattern scaling coefficients derived from CMIP6 GCMs (Fig. S5, S6), and adjust the exposure-response function accordingly (Methods). Following other work (9), our approach to adaptation thus relies on extrapolating current heterogeneity in exposure-response functions into the future and assumes that future societies will continue to adapt with the same pattern as has been recently observed.

Across the five illustrative events we study, allowing such adaptation reduces peak mortality by only 11% on average (Fig. 4). For example, mortality during 2003 meteorological conditions in a 3 °C year is projected to be 31,620 in our main projections and 28,092 when allowing additional adaptation. The with-adaptation peak mortality from the most

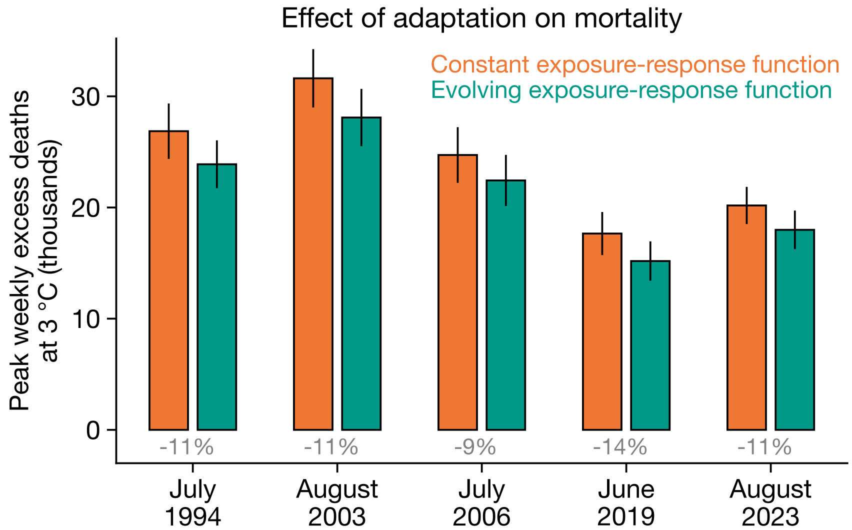

Figure 4: Limited potential to reduce heat mortality by scaling up observed adaptation. Each bar shows the peak weekly mortality at 3 °C for each set of meteorological conditions. The orange bars show our main calculation (i.e., the peak of the 3 °C curve in Fig. 3), which incorporates existing adaptation through spatial heterogeneity in exposure-response functions. The green bars show the same calculation after accounting for additional future climate adaptation by allowing exposure-response curves to evolve with future climate change (Methods). Bar heights shows average projections and error bars show 95% range. Gray text denotes the percent reduction in mortality from additional future adaptation.

extreme event (2003) remains larger even than the no-adaptation peak mortality of the other events. These results imply that there is limited potential for currently deployed adaptation approaches to reduce the mortality impacts of these extreme climate events.

Discussion and Conclusion

Several caveats and analytical choices should be considered when evaluating these results. For instance, we use total all-age mortality rather than age-stratified rates to maximize the coverage of our data (Methods). Under-65 and over-65 mortality rates appear to respond similarly to heat in Europe (Fig. S7), so this choice should not substantially affect our results. Relatedly, we calculate excess mortality relative to 2015-2019 average mortality rates, so the numbers we report are benchmarked to near-present population. Given these choices, large future shifts in population, age structure, or other demographics could alter the total death toll of extreme heat events and their demographic distribution (41). However, given that Europe's population is only expected to rise by ∼1% over the next several decades before slightly declining later in the century (42), these trends should only slightly affect our results. Further, given that population aging in Europe may amplify future heat sensitivity (13, 41), our estimates are likely conservative.

In addition, our projections are conditional on weather patterns that are rare by definition. It is possible that these mortality events would not take place even with substantial warming if the corresponding meteorological conditions do not occur again. On the other hand, even more severe events could be produced if novel weather patterns occur due to the interaction of internal variability and global warming. Further, our results reveal a latent potential for meteorological patterns that did not cause significant excess mortality in the past to do so in the future if they occur at higher GMTs. For example, at equivalent GMT, the July 1994 meteorological conditions are predicted to produce the highest cumulative mortality and second highest peak mortality of any of the illustrative events (Table S1).

This finding also illustrates the reason that we avoid calculating "observed" mortality from each event at the time that it actually occurred. Each event occurred at a different level of global warming and potentially with a different degree of human adaptation to heat. Indeed, in other recent work, we show that the heat-mortality relationship in France is very different before 2003, meaning that calculating "observed" heat mortality in 2003 may require a more sophisticated exposure-response function (43). The benefit of our forward-looking approach is that we can analyze a range of known meteorological conditions at the same GMT levels, allowing standardized comparisons between historically different events with a single exposure-response function that reflects recent adaptation.

To further contextualize the magnitude of the death tolls we calculate, we compare them to weekly confirmed COVID-19 deaths across the same regions of Europe. For example, the most severe 10% of weeks of COVID-19 had between 27,900 and 34,100 confirmed deaths. At 3 °C, the weekly death toll from 2003-like conditions is comparable to these peak weeks of COVID-19, and at 4 °C, the weekly death tolls of 1994-, 2003-, and 2006-like conditions would exceed even the single worst week of COVID-19 in Europe (Fig. S8).

It is notable that our results suggest limited potential for the existing patterns and forms of adaptation to mitigate these mass mortality events. In our analysis, this result may occur because although warmer regions in Europe have higher MMTs, they also have steeper exposure-response curves above those MMTs (Fig. 2). More broadly, it is consistent with other work emphasizing that heat still poses a major public health threat despite putative progress since the deadly 2003 summer (44–46). However, our approach to adaptation is based on extrapolating observed spatial heterogeneity in exposure-response functions. If novel technologies or policies emerge more quickly or in a different pattern than past adaptation, mortality could be reduced further. Additionally, accounting for further changes in other characteristics such as income may reveal additional opportunities for adaptation.

Several studies have calculated large mortality impacts of the hot European summers of 2022 and 2023 (32–34). Our work differs from theirs by incorporating further global warming, and therefore potentially greater mortality. For example, Ballester et al. (32) show a peak of 11,637 weekly heat-related deaths in 2022 in a similar sample of European regions. Even at current global temperatures of 1.5 °C, our results show that either 1994 or 2003 meteorological conditions would generate more than 14,038 and 17,340 weekly excess deaths at their peak, respectively, larger than the 2022 peak. At higher GMT and 2003-like meteorological conditions, our predicted peak mortality totals are 84% (2 °C) and 172% (3 °C) greater than in 2022. However, we caution that the methods of these papers and ours differ in some analytical choices such as the definition of the counterfactual.

Overall, our results reveal a substantial death toll from potential future extreme heat events in Europe. These results are based on observed meteorological patterns that occurred in the historical record combined with plausible 21st-century global temperature anomalies, making them physically realistic storylines of potential high-magnitude heat events. Additionally, we specifically distinguish between the contributions of climate change and natural variability conditional upon these realistic meteorological patterns, revealing that climate change is already a dominant contributor to mortality during extreme heat events, and its contribution could exceed 70-80% of deaths at higher levels of warming (Table S2).

Our characterization of specific, plausible high-magnitude outcomes is an important complement to existing heat mortality projections and can help inform health system preparedness and planning. Most importantly, our results demonstrate that even if global temperatures are stabilized, substantial and novel adaptation measures may be required to reduce the continent-wide threat of extreme heat to population health.

Methods

Data

We draw weekly mortality data from the Eurostat database (data code "demo_r_mweek3"). Different regions make data available over different time periods; we limit our analysis to 2015-2019 to match the most common period of data availability, following other work (32). Where possible, we use all-age, all-sex mortality rates from NUTS3 (third administrative level below country) regions, except in Germany, where we only have these data at the NUTS1 level. This yields a total of 924 regions with continuous mortality rate data over 2015-2019. Age-group-specific rates (0-64 and 65+) are available for only a slightly smaller number of regions (N = 908), so we use all-age rates to maximize coverage in our preferred specification.

Our historical climate data come from the E-OBS station-based dataset (47) and the ERA5 reanalysis (48). We use E-OBS daily surface temperature for the mortality calculations and ERA5 for the machine learning applications and maps in Fig. 1. E-OBS data are spatially averaged to the appropriate NUTS regions, weighting grid cells within regions by the population of each grid cell.

Counterfactual extreme heat events

We use a machine learning architecture recently developed and validated by Trok et al. (35) to produce counterfactual versions of historical extreme heat events. This approach trains convolutional neural networks (CNNs) on an ensemble of GCM realizations, with the goal of predicting daily mean temperature over a specified region given daily meteorological conditions and the annual global mean temperature (GMT).

The predictors for each day are daily sea level pressure, daily geopotential height at the 700-, 500-, and 250-mb levels, daily soil moisture between 0 and 10 cm, the calendar day, and the GMT anomaly over the previous 12 months. Prior to training, the meteorological predictors are detrended with respect to the grid cell, calendar day, and GMT, and then standardized by subtracting the grid-cell calendar-day mean and dividing by the grid-cell calendar-day standard deviation (35). The detrended and standardized surface pressure, geopotential height, and soil moisture are the factors we refer to as "meteorological conditions" throughout the text. Using detrended and standardized anomalies in this process means that these meteorological conditions explain day-to-day variation in temperature, but do not contain the signal of global warming.

In our experimental setup, we follow Trok et al. (35) in first training the CNNs on five realizations each of two GCMs (CanESM5 and UKESM1-0-LL) that provide sufficient daily data, over 1850-2100 using the historical and SSP5-8.5 emissions scenarios. We then apply the model to predict daily temperatures using predictor data from the ERA5 reanalysis. One set of predictions uses the observed GMT time series, whereas the other sets use counterfactual GMT values but maintain the other daily predictors from the reanalysis. The result is a set of counterfactual temperature time series that maintain realistic day-to-day weather conditions but vary according to the annual GMT anomaly.

We use a "delta" method to apply the CNN predictions to E-OBS gridded observations. For each day in the event of interest, we take the difference between the counterfactual CNN predictions on that day and the original CNN predictions for that day using the actual GMT. We then apply these deltas to the E-OBS observed data for that day to calculate counterfactual daily time series. Finally, we aggregate these counterfactual gridded daily temperature data into averages at the NUTS region level as with the original observations.

In Trok et al. (35), the CNN architecture was trained to predict temperature in regions chosen for their relevance to specific historical extremes. In our application, we would like to apply these predictions to a set of events, each with slightly different spatial footprints. We therefore train the CNNs to predict temperature change on land in each of three regions as defined by the Intergovernmental Panel on Climate Change (IPCC): the Mediterranean (MED), Western and Central Europe (WCE), and Northern Europe (NEU) (49). The events manifest differently in each of these regions, with temperatures generally highest in the Mediterranean region and lowest in Northern Europe (Fig. S3). We then apply the deltas for each region uniformly to the grid cells within each region.

Finally, we perform each of the above steps three times, each time with a different random seed to account for random differences in model training. This yields three different CNN predictions for each day, GMT level, and IPCC region.

Exposure-response functions

We use panel regression with fixed effects to measure the causal effect of temperature on mortality across Europe. This widely used approach (9, 10, 50–52) involves regressing mortality rates on a nonlinear function of temperature, along with vectors of intercepts (fixed effects) that non-parametrically remove seasonal or annual average factors separately for each region.

We also account for heterogeneity across regions by interacting temperature with each region's 2000-2019 average temperature, allowing the temperature exposure-response curve to vary based on a region's long-term climate. This approach leverages cross-sectional variation in temperature to assess societal adaptation to extreme heat, in effect asking whether the same temperature level has a different effect in a region that is warmer on average than a region that is cooler on average. We emphasize that cross-sectional variation is less amenable to causal identification since there may be other factors (e.g., income, demographics) that are correlated with both average temperature and heat sensitivity. Nevertheless, assessing heterogeneity by mean temperature is a well-established strategy for identifying present and future climate adaptation (9, 53–56), so we adopt it here while acknowledging the potential for additional relevant axes of heterogeneity. Our approach is also similar to multi-stage methods that have been used in other recent papers on heat mortality to estimate spatial variation in exposure-response functions (e.g., 11, 57, 58), though we run a single regression that accommodates variations across regions rather than pooling time series regressions from separate regions.

Specifically, we estimate the following regression relating contemporaneous and lagged temperature vectors $\mathbf{T}$ to log mortality rates M in region i, week w, and year y with Ordinary Least Squares:

$$M_{iwy} = \sum_{j=0}^{L} \left[f(\mathbf{T}_{i(w-j)y}) + f(\mathbf{T}_{i(w-j)y}) \times \overline{T}_i \right] + \mu_{iy} + \delta_{iw} + \epsilon_{iwy} \tag{1}$$

The region-year fixed effects μ_{iy} and region-week fixed effects δ_{iw} remove the influence of long-term trends and seasonal cycles that could confound the temperature-mortality interaction, and do so separately for each region. The $\overline{T}_i$ term denotes the 2000-2019 mean temperature in each region i. We estimate distributed lag models that sum the impact on mortality of contemporaneous and lagged temperature exposure, with j indexing weekly lags. As described below, our main model uses 3 weeks of lagged temperatures.

A key consideration in this estimation is that mortality rates are provided at the weekly scale but temperature extremes can impact mortality rates on daily timescales. We require a strategy that preserves daily nonlinearities while matching the weekly scale of the mortality data. We thus follow previous work (9) and sum the daily mean temperature from each day d within week w after a fourth-order nonlinear transformation has been applied to each day's temperature:

$$f(\mathbf{T}_{iwy}) = \beta_1 \sum_{d=1}^{7} T_{iw(d)y} + \beta_2 \sum_{d=1}^{7} T^2_{iw(d)y} + \beta_3 \sum_{d=1}^{7} T^3_{iw(d)y} + \beta_4 \sum_{d=1}^{7} T^4_{iw(d)y} \tag{2}$$

We estimate independent coefficients for each of the summed polynomial terms in Eqn 2. Because weekly mortality rates are the sum of daily mortality rates (given constant population), calculating the effects of daily sums preserves the nonlinear effect of each individual day on weekly mortality rates. We use daily mean temperature following earlier work (9), but using daily maximum or daily minimum temperatures yields only small differences in exposure-response functions (Fig. S7).

Regressions are weighted by each region's population. We estimate uncertainty by bootstrap resampling 500 times, blocked by region, meaning we preserve within-region autocorrelation when resampling (akin to clustering standard errors by region).

We use lags in the regression to incorporate delayed effects of temperature. These delayed effects could arise simply due to additional mortality if people die several days after heat exposure. They could also manifest as "displacement" or "harvesting," where mortality is abnormally low after heat waves since the heat accelerated the deaths of people who would have died soon regardless of the heat. Indeed, we do observe some displacement following the events (Fig. 3): the lag-2 and lag-3 regression coefficients are negative (Fig. S9). We use three lags in our main analysis following earlier work (32), but re-estimating the model using 6 lags yields similar results, with potentially slightly more displacement in additional weeks (Fig. S9).

Calculating counterfactual mortality

Our central calculation compares a series of abnormally hot days at a given GMT level to a long-term mean baseline without global warming (Fig. S2). We perform this calculation by applying the exposure-response function (Fig. 2) to the temperature time series in each region and comparing it to the same prediction when applied to the baseline time series. Because our outcome is log mortality, the difference between each prediction yields a percent change in mortality due to experiencing the temperature at each GMT instead of the baseline temperature. We then multiply this percent change by the average number of deaths in each region observed over 2015-2019 to calculate the additional mortality from each event. Because these deaths are relative to an underlying baseline number of deaths, we refer to them as "excess deaths" or "excess mortality."

Note that we generally refer to the events predicted by the machine learning method for different GMT anomalies as "counterfactual" events, whereas we use "baseline" to refer to a long-term average without the event.

One key methodological question in this procedure is the construction of the baseline temperature from which excess deaths are calculated. We are interested in the total number of excess deaths associated with each event, not just those caused by climate change. We therefore construct a baseline which does not include either climate change or extreme heat events. This is done in two steps:

1. We use the machine learning approach described above to construct counterfactual estimates for every summer day between 1980-2023 at 0 °C. We subtract the "delta" from this procedure from the E-OBS observations to construct a counterfactual dataset at 0 °C over the entire observational time period (i.e., not just for each event). This yields a 44-year counterfactual temperature time series for each region that includes daily weather variability and extreme heat events, but not the influence of climate change.

2. We then take the long-term average across 1980-2023 from this counterfactual time series for each calendar day in each region.

The result of this calculation is an estimate of the average seasonal cycle in each region at

0 °C. Because the influence of climate change was removed from these observed temperatures, this baseline does not include global warming, and because it was averaged over all years for each calendar day, it does not include deviations from the seasonal cycle (i.e., it does not include extreme heat events). The black dashed line in Fig. S2 shows the Europe-wide average of these baseline temperatures over the time period of each event.

We quantify uncertainty in the final excess deaths totals with Monte Carlo simulations. In each of 500 iterations, we randomly sample one of the bootstrap samples of the regression estimates and one of the three CNNs. When we incorporate adaptation (see below), we also sample one of the pattern scaling coefficients for each region in each iteration.

Adaptation to climate change

Our regression approach (Eqn. 1) accounts for current adaptation to heat by allowing exposures-response functions to vary according to regions' 2000-2019 mean temperature. This approach assumes that vulnerability to temperature during the 2015-2019 data period fully reflects efficient levels of adaptation investment (such as installing air conditioning, taking indoor jobs rather than working outdoors, or implementing heat action plans in cities), justifiable based on longer-term (2000-2019) exposures. In the future, especially in light of rising incomes, we might expect additional such actions, which could reduce the death toll that we project.

We project future adaptation under the assumption that changes in regions' long-run mean temperatures directly translate into additional adaptation actions. We thus require an estimate of future long-run (i.e., 20-year) mean temperature in each region, with which to adjust the exposure-response functions (Fig. 2). However, our approach predicts event intensity using annual global temperature, a quantity which does not directly translate into local mean temperatures over the previous 20 years. Therefore, we adopt a pattern scaling approach, following IPCC AR6 WGI Chapter 4 (59), to simulate increased 20-year mean temperatures in each European subnational district depending on a given annual GMT. We use 27 models from the sixth phase of the Coupled Model Intercomparison Project (60), spanning the historical and SSP3-7.0 experiments (61). For each year, we calculate GMT anomalies (relative to 1850-1900) and local mean temperature anomalies over the previous 20 years for each European region (relative to 2000-2019). For example, for 2069 in the region that encompasses Berlin, we have the GMT change in 2069 and the regional mean temperature change over 2049-2068. The relationship between these two quantities is generally linear (Fig. S5), and yields a coherent spatial pattern across Europe (Fig. S6) that is reflective of the forced response (59).

In our Monte Carlo simulations of event mortality, we pool all model-years for these two quantities from 2020-2100, randomly sample a set of these model-years with replacement, then use the region-specific intercepts and slopes from this random sample. Then, in each calculation of event mortality at each annual GMT, we predict each region's additional mean temperature change (relative to 2000-2019) given the GMT, slope, and intercept, and add this additional temperature change to the region's 2000-2019 mean temperature. This new mean temperature value is then used in the calculation of each region's mortality from their exposure-response functions (Fig. 2), allowing the exposure-response functions to evolve in the future given a prediction (with uncertainty) of changing local mean temperatures.

Finally, as a sensitivity test, we compare with an alternative stylized approach where we simply warm each European region's mean temperature by the same amount as the GMT level for each event. That is, the GMT in 2000-2019 was approximately 1 °C relative to 1850-1900, so we add 1 additional degree to each region's mean temperature for the events at 2 °C, 2 additional degrees to each region's mean temperature for the events at 3 °C, and so on. This stylized approach yields qualitatively similar results, reducing the average event mortality by 12.5% compared to 11% in our main approach (Fig. S10).

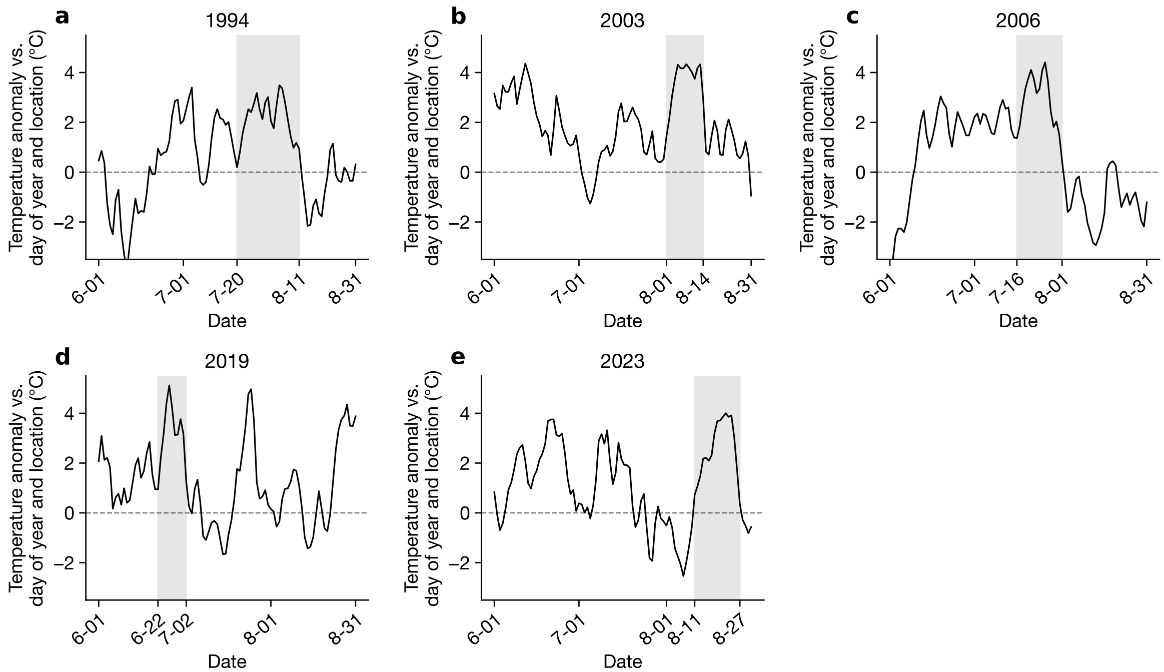

Figure S1: Temperature anomalies for selected events. Each plot shows temperatures anomalies from June through August, calculated as the population-weighted mean across all European subnational regions for which we have mortality data. Anomalies are calculated with respect to each region and day of year. Gray shading shows the periods that we define as each event.

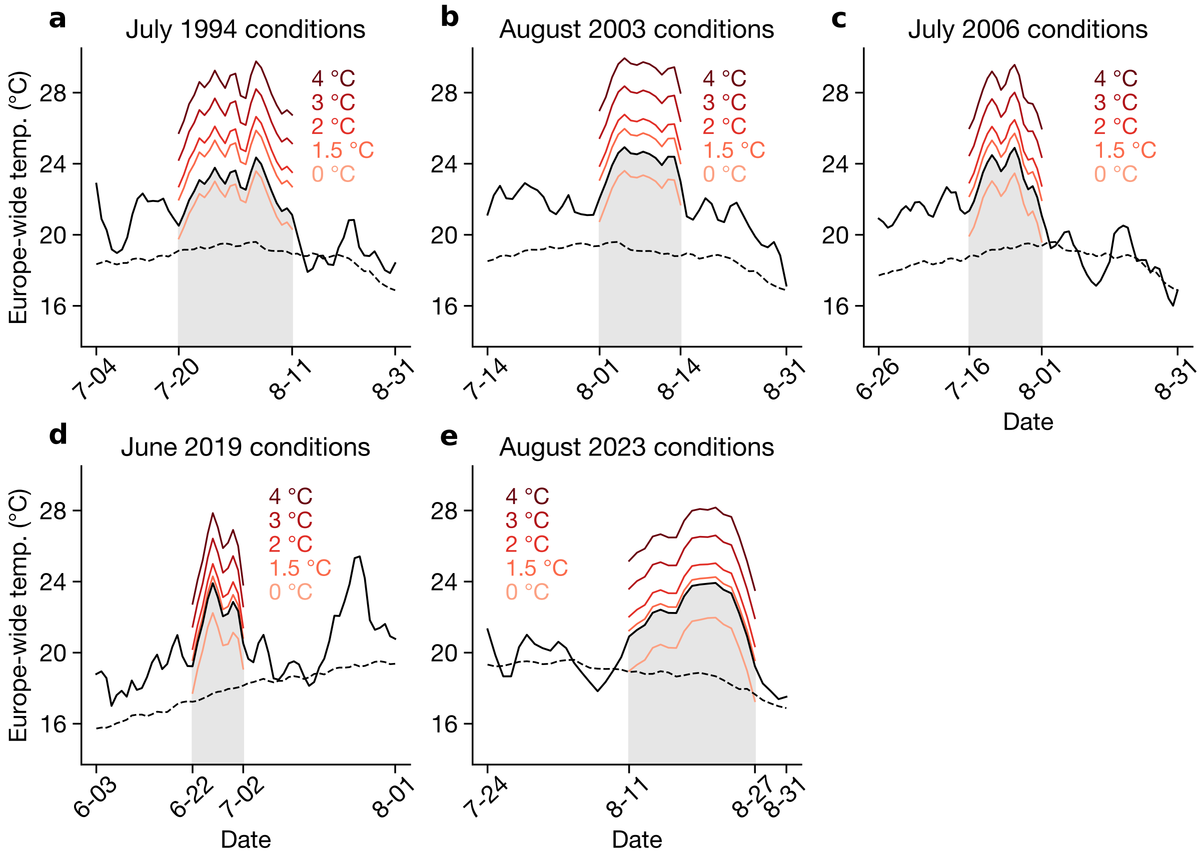

Figure S2: Actual and counterfactual Europe-wide temperatures. Time series of observed (black solid line), baseline without warming or heat waves (black dashed line), and counterfactual event (red colored lines) temperatures across Europe. Europe-wide temperatures are calculated as the population-weighted average across all subnational regions for which we have temperature data. Gray shading denotes the periods we define as the "events"; these dates are originally defined using Europe-wide temperature anomalies (Fig. S1) but are shown here for clarity.

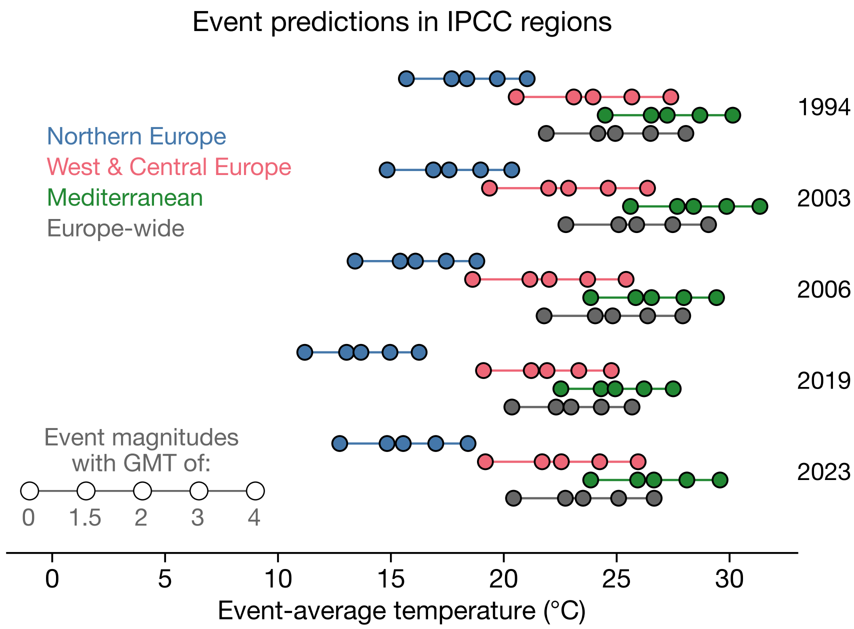

Figure S3: Temperature for each event in IPCC AR6 regions. As in the lower points in Fig. 2, but for each of the three IPCC regions for which we train the CNNs.

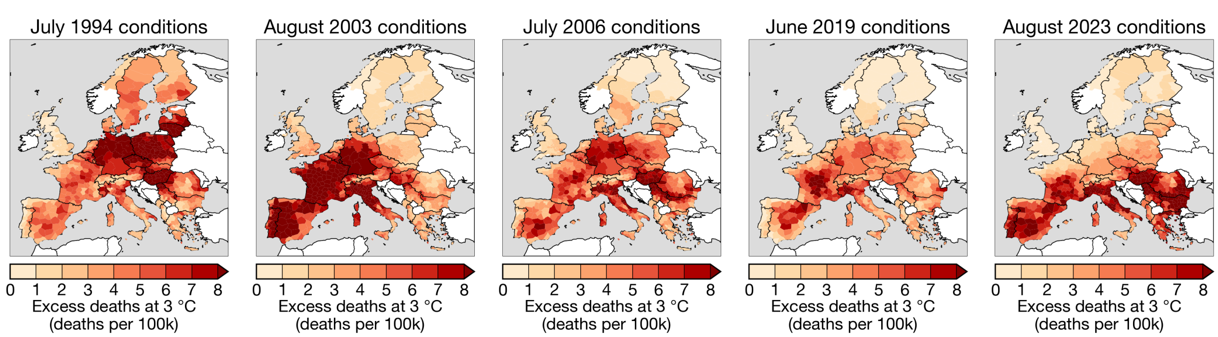

Figure S4: Regional mortality rates during extreme heat events. Each panel shows the regional mortality rate, in deaths per 100,000 population, in the peak week of each counterfactual heat wave at 3 °C. Peak weeks are defined as the week of maximum Europe-wide excess deaths (i.e., maximum point in Fig. 3). White regions are those for which we do not have population or mortality data.

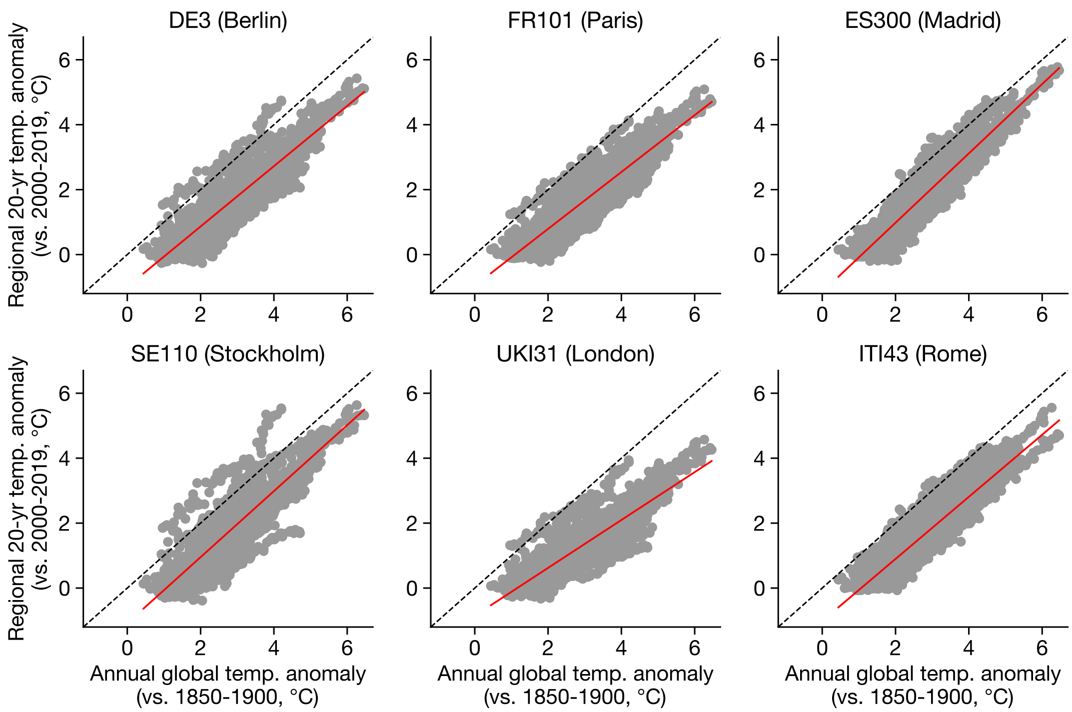

Figure S5: Examples of pattern-scaling local mean temperature as a function of global annual temperature. Each panel shows the relationship between annual global mean temperature (relative to 1890-1900) and a European region's mean temperature in the 20 prior years (relative to 2000-2019). Gray dots show all model-years using a sample of 27 GCMs over 2020-2100, red line shows linear best-fit line, and black dashed line is the 1:1 line.

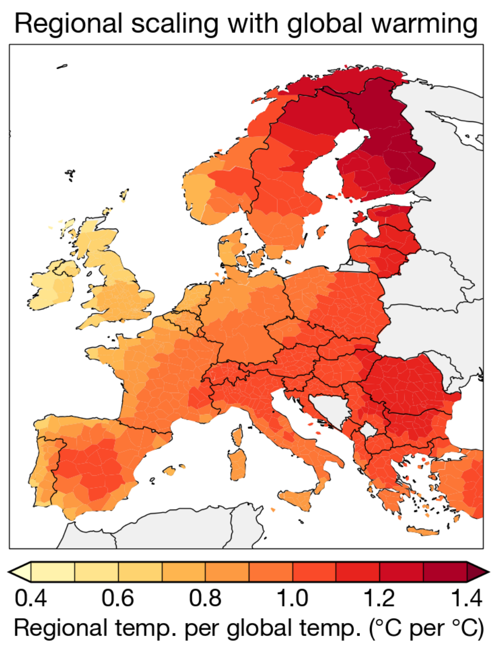

Figure S6: Pattern scaling coefficients across European regions. Linear coefficient between annual global temperature and regional mean temperature in the previous 20 years. Coefficients are averaged across 100 random samples of pooled model-year populations (i.e., gray dots in Fig. S5).

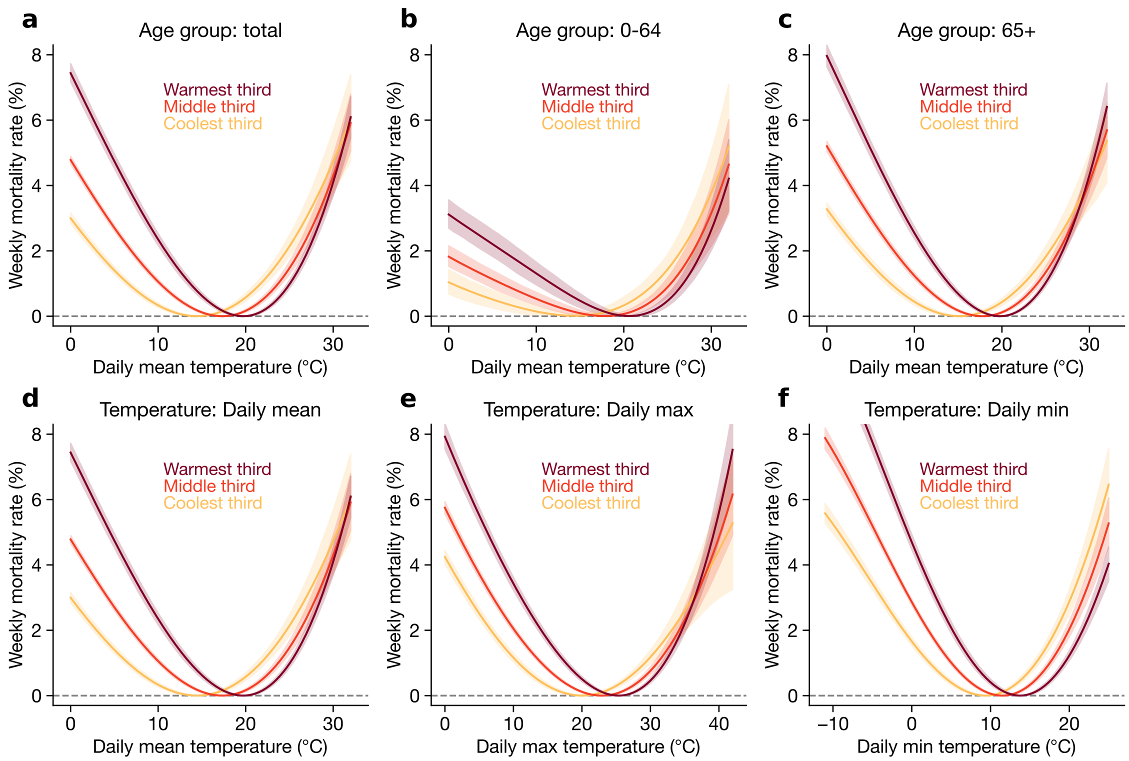

Figure S7: Alternative exposure-response curves. Panel (a) shows our main exposure-response function, which uses total all-age mortality (same as Fig. 2). Panels (b) and (c) show the same regression specification using under-65 (b) and 65-and-over (c) mortality. Panel (d) again shows our main exposure-response function, which uses daily mean temperature. Panels (e) and (f) show the same specification using daily maximum (e) and daily minimum (f) temperature. Note that the x-axes are scaled differently in (e) and (f) to account for the different observed ranges of the temperature metrics.

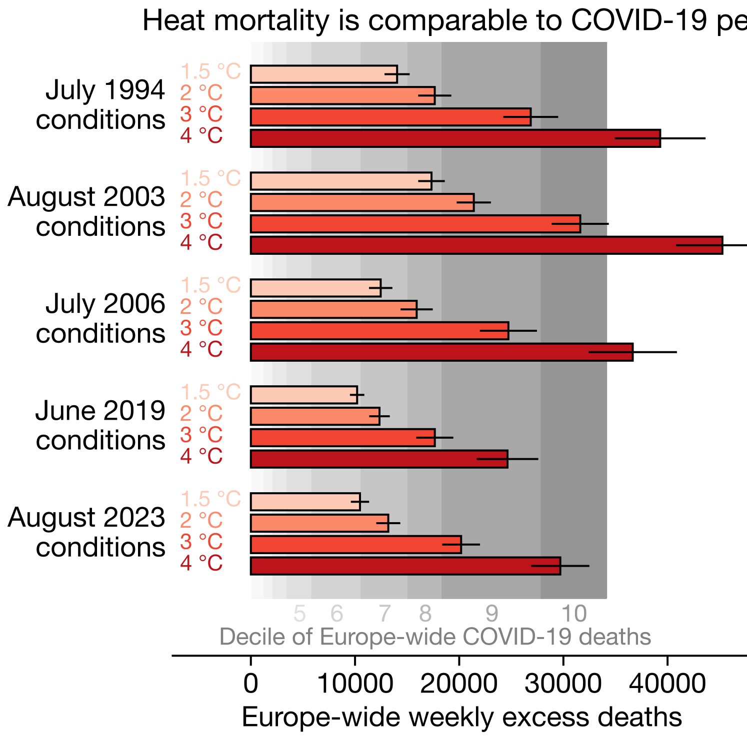

Figure S8: Peak heat mortality compared to peak COVID-19 mortality. Red bars show peak weekly mortality from each set of meteorological conditions (i.e., the peaks of the curves in Fig. 3). Bar widths show mean projection and error bars show 95% range. Gray shading shows the deciles of Europe-wide weekly confirmed COVID-19 deaths. For example, the darkest gray shading shows the range of the top 10% of weeks of COVID-19 deaths, the second-to-darkest shading shows the range of the top 10-20% of weeks, and so on.

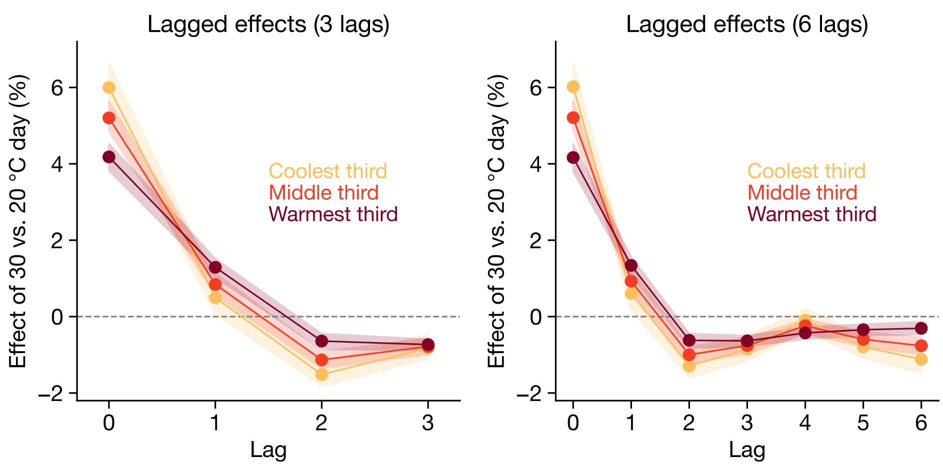

Figure S9: Effect of a hot day across lags. Both panels show the mortality effect of a 30 °C day relative to a 20 °C day, at a series of lags relative to the week of mortality. Lag 0 means contemporaneous temperature, lag 1 means temperature the week before, and so on. In our main analysis, we use 3 lags (left panel), but we also test a model with 6 lags (right panel).

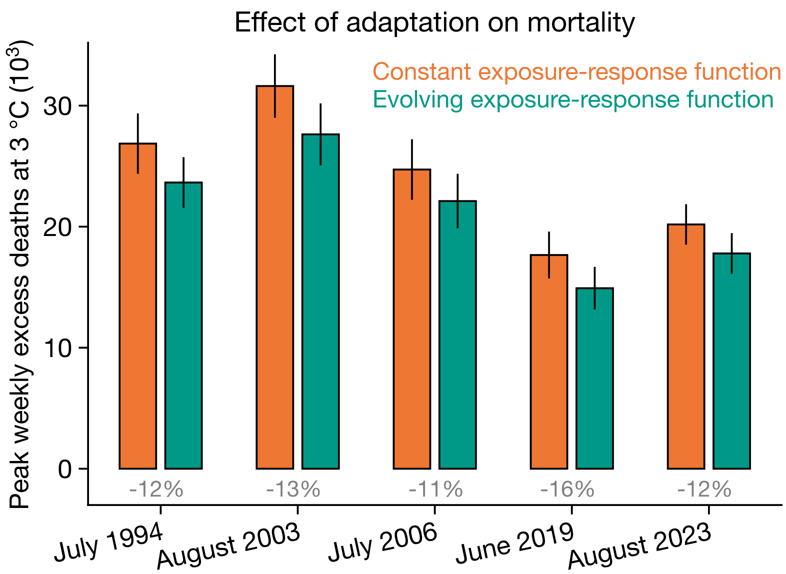

Figure S10: Adaptation when simply scaled by GMT. As in Fig. 4, but for a version of adaptation where we simply assume that the mean temperature in each European region warms the same amount as the annual GMT level used for each event simulation.

Event	GMT	Peak mortality	Cumulative mortality
July 1994	1.5	14038	31516
July 1994	2.0	17652	40164
July 1994	3.0	26865	62183
July 1994	4.0	39295	91854
August 2003	1.5	17340	25923
August 2003	2.0	21401	32344
August 2003	3.0	31620	48457
August 2003	4.0	45266	69846
July 2006	1.5	12463	21011
July 2006	2.0	15917	27035
July 2006	3.0	24721	42305
July 2006	4.0	36658	62820
June 2019	1.5	10200	10350
June 2019	2.0	12346	12861
June 2019	3.0	17657	19222
June 2019	4.0	24635	27716
August 2023	1.5	10475	17649
August 2023	2.0	13191	22710
August 2023	3.0	20183	35774
August 2023	4.0	29704	53544

Table S1: Europe-wide mortality for each event. Each row shows the maximum weekly excess deaths ("peak") and cumulative excess deaths for each event at each global mean temperature ("GMT"). We note that because the events differ slightly in their durations (Fig. S1), peak single-week mortality is more directly comparable across events than cumulative mortality.

Event	GMT	Peak mortality from warming	Percent from warming
July 1994	1.5	7829	56%
July 1994	2.0	11443	65%
July 1994	3.0	20656	77%
July 1994	4.0	33086	84%
August 2003	1.5	8874	51%
August 2003	2.0	12934	60%
August 2003	3.0	23154	73%
August 2003	4.0	36799	81%
July 2006	1.5	7377	59%
July 2006	2.0	10831	68%
July 2006	3.0	19636	79%
July 2006	4.0	31572	86%
June 2019	1.5	4835	47%
June 2019	2.0	6980	57%
June 2019	3.0	12292	70%
June 2019	4.0	19269	78%
August 2023	1.5	5646	54%
August 2023	2.0	8362	63%
August 2023	3.0	15354	76%
August 2023	4.0	24875	84%

Table S2: Climate change-driven mortality for each event. The "peak mortality from climate change" row shows the peak weekly excess deaths for each event at each GMT relative to the peak of the event at 0 °C, meaning only the component of mortality due to anthropogenic intensification of the event. The "percent from warming" column shows the percent of overall peak mortality (Table S1) due to climate change

References

[1] Gerald A Meehl and Claudia Tebaldi. More intense, more frequent, and longer lasting heat waves in the 21st century. *Science*, 305(5686):994–997, 2004.

[2] Stefan Rahmstorf and Dim Coumou. Increase of extreme events in a warming world. *Proceedings of the National Academy of Sciences*, 108(44):17905–17909, 2011.

[3] EM Fischer, Sebastian Sippel, and Reto Knutti. Increasing probability of record-shattering climate extremes. *Nature Climate Change*, 11(8):689–695, 2021.

[4] Noah S Diffenbaugh, Deepti Singh, Justin S Mankin, Daniel E Horton, Daniel L Swain, Danielle Touma, Allison Charland, Yunjie Liu, Matz Haugen, Michael Tsiang, et al. Quantifying the influence of global warming on unprecedented extreme climate events. *Proceedings of the National Academy of Sciences*, 114(19):4881–4886, 2017.

[5] Kristie L Ebi, Anthony Capon, Peter Berry, Carolyn Broderick, Richard de Dear, George Havenith, Yasushi Honda, R Sari Kovats, Wei Ma, Arunima Malik, et al. Hot weather and heat extremes: health risks. *The Lancet*, 398(10301):698–708, 2021.

[6] Daniela IV Domeisen, Elfatih AB Eltahir, Erich M Fischer, Reto Knutti, Sarah E Perkins-Kirkpatrick, Christoph Schär, Sonia I Seneviratne, Antje Weisheimer, and Heini Wernli. Prediction and projection of heatwaves. *Nature Reviews Earth & Environment*, 4(1):36–50, 2023.

[7] Jean-Marie Robine, Siu Lan K Cheung, Sophie Le Roy, Herman Van Oyen, Clare Griffiths, Jean-Pierre Michel, and François Richard Herrmann. Death toll exceeded 70,000 in europe during the summer of 2003. *Comptes Rendus. Biologies*, 331(2):171–178, 2008.

[8] Solomon Hsiang, Robert Kopp, Amir Jina, James Rising, Michael Delgado, Shashank Mohan, DJ Rasmussen, Robert Muir-Wood, Paul Wilson, Michael Oppenheimer, et al. Estimating economic damage from climate change in the united states. *Science*, 356(6345):1362–1369, 2017.

[9] Tamma Carleton, Amir Jina, Michael Delgado, Michael Greenstone, Trevor Houser, Solomon Hsiang, Andrew Hultgren, Robert E Kopp, Kelly E McCusker, Ishan Nath, et al. Valuing the global mortality consequences of climate change accounting for adaptation costs and benefits. *The Quarterly Journal of Economics*, 137(4):2037–2105, 2022.

[10] Olivier Deschênes and Michael Greenstone. Climate change, mortality, and adaptation: Evidence from annual fluctuations in weather in the US. *American Economic Journal: Applied Economics*, 3(4):152–85, 2011.

[11] Antonio Gasparrini, Yuming Guo, Francesco Sera, Ana Maria Vicedo-Cabrera, Veronika Huber, Shilu Tong, Micheline de Sousa Zanotti Stagliorio Coelho, Paulo Hilario Nascimento Saldiva, Eric Lavigne, Patricia Matus Correa, et al. Projections of temperature-related excess mortality under climate change scenarios. *The Lancet Planetary Health*, 1(9):e360–e367, 2017.

[12] Ana Maria Vicedo-Cabrera, Yuming Guo, Francesco Sera, Veronika Huber, Carl-Friedrich Schleussner, Dann Mitchell, Shilu Tong, Micheline de Sousa Zanotti Stagliorio Coelho, Paulo Hilario Nascimento Saldiva, Eric Lavigne, et al. Temperature-related mortality impacts under and beyond paris agreement climate change scenarios. *Climatic Change*, 150:391–402, 2018.

[13] David García-León, Pierre Masselot, Malcolm N Mistry, Antonio Gasparrini, Corrado Motta, Luc Feyen, and Juan-Carlos Ciscar. Temperature-related mortality burden and projected change in 1368 european regions: a modelling study. *The Lancet Public Health*, 9(9):e644–e653, 2024.

[14] Lisa Patel, Kathryn C Conlon, Cecilia Sorensen, Samia McEachin, Kari Nadeau, Khyati Kakkad, and Kenneth W Kizer. Climate change and extreme heat events: how health systems should prepare. *NEJM Catalyst Innovations in Care Delivery*, 3(7):CAT–21, 2022.

[15] Kristie L Ebi, Peter Berry, Katie Hayes, Christopher Boyer, Samuel Sellers, Paddy M Enright, and Jeremy J Hess. Stress testing the capacity of health systems to manage climate change-related shocks and stresses. *International Journal of Environmental Research and Public Health*, 15(11):2370, 2018.

[16] Claudia Gessner, Erich M Fischer, Urs Beyerle, and Reto Knutti. Very rare heat extremes: quantifying and understanding using ensemble reinitialization. *Journal of Climate*, 34(16):6619–6634, 2021.

[17] Theodore G Shepherd. Atmospheric circulation as a source of uncertainty in climate change projections. *Nature Geoscience*, 7(10):703–708, 2014.

[18] Samuel Lüthi, Christopher Fairless, Erich M Fischer, Noah Scovronick, Ben Armstrong, Micheline De Sousa Zanotti Stagliorio Coelho, Yue Leon Guo, Yuming Guo, Yasushi Honda, Veronika

Huber, et al. Rapid increase in the risk of heat-related mortality. *Nature Communications*, 14 (1):4894, 2023.

[19] Efi Rousi, Kai Kornhuber, Goratz Beobide-Arsuaga, Fei Luo, and Dim Coumou. Accelerated western european heatwave trends linked to more-persistent double jets over eurasia. *Nature Communications*, 13(1):3851, 2022.

[20] Jitendra Singh, Sebastian Sippel, and Erich M Fischer. Circulation dampened heat extremes intensification over the midwest usa and amplified over western europe. *Communications Earth & Environment*, 4(1):432, 2023.

[21] Robert Vautard, Julien Cattiaux, Tamara Happé, Jitendra Singh, Rémy Bonnet, Christophe Cassou, Dim Coumou, Fabio D'andrea, Davide Faranda, Erich Fischer, et al. Heat extremes in western europe increasing faster than simulated due to atmospheric circulation trends. *Nature Communications*, 14(1):6803, 2023.

[22] Kai Kornhuber, Samuel Bartusek, Richard Seager, Hans Joachim Schellnhuber, and Mingfang Ting. Global emergence of regional heatwave hotspots outpaces climate model simulations. *Proceedings of the National Academy of Sciences*, 121(49):e2411258121, 2024.

[23] Theodore G Shepherd, Emily Boyd, Raphael A Calel, Sandra C Chapman, Suraje Dessai, Ioana M Dima-West, Hayley J Fowler, Rachel James, Douglas Maraun, Olivia Martius, et al. Storylines: an alternative approach to representing uncertainty in physical aspects of climate change. *Climatic Change*, 151:555–571, 2018.

[24] Rowan T Sutton. Climate science needs to take risk assessment much more seriously. *Bulletin of the American Meteorological Society*, 100(9):1637–1642, 2019.

[25] Jana Sillmann, Theodore G Shepherd, Bart Van Den Hurk, Wilco Hazeleger, Olivia Martius, Julia Slingo, and Jakob Zscheischler. Event-based storylines to address climate risk. *Earth's Future*, 9(2):e2020EF001783, 2021.

[26] Anne Fouillet, Grégoire Rey, Vérène Wagner, Karine Laaidi, Pascal Empereur-Bissonnet, Alain Le Tertre, Philippe Frayssinet, Pierre Bessemoulin, Françoise Laurent, Perrine De Crouy-Chanel, et al. Has the impact of heat waves on mortality changed in France since the European heat wave of summer 2003? A study of the 2006 heat wave. *International Journal of Epidemiology*, 37(2):309–317, 2008.

[27] Daniel E Horton, Nathaniel C Johnson, Deepti Singh, Daniel L Swain, Bala Rajaratnam, and Noah S Diffenbaugh. Contribution of changes in atmospheric circulation patterns to extreme temperature trends. *Nature*, 522(7557):465, 2015.

[28] Erich M Fischer, Sonia I Seneviratne, Daniel Lüthi, and Christoph Schär. Contribution of land-atmosphere coupling to recent European summer heat waves. *Geophysical Research Letters*, 34 (6), 2007.

[29] Diego G Miralles, Adriaan J Teuling, Chiel C Van Heerwaarden, and Jordi Vila-Guerau De Arellano. Mega-heatwave temperatures due to combined soil desiccation and atmospheric heat accumulation. *Nature Geoscience*, 7(5):345–349, 2014.

[30] Abderrezak Bouchama and James P Knochel. Heat stroke. *New England Journal of Medicine*, 346(25):1978–1988, 2002.

[31] Nikolaos Christidis, Gareth S Jones, and Peter A Stott. Dramatically increasing chance of extremely hot summers since the 2003 European heatwave. *Nature Climate Change*, 5(1): 46–50, 2015.

[32] Joan Ballester, Marcos Quijal-Zamorano, Raúl Fernando Méndez Turrubiates, Ferran Pegenaute, François R Herrmann, Jean Marie Robine, Xavier Basagaña, Cathryn Tonne, Josep M Antó, and Hicham Achebak. Heat-related mortality in Europe during the summer of 2022. *Nature medicine*, 29(7):1857–1866, 2023.

[33] Elisa Gallo, Marcos Quijal-Zamorano, Raúl Fernando Méndez Turrubiates, Cathryn Tonne, Xavier Basagaña, Hicham Achebak, and Joan Ballester. Heat-related mortality in Europe during 2023 and the role of adaptation in protecting health. *Nature Medicine*, pages 1–5, 2024.

[34] Thessa M Beck, Dominik L Schumacher, Hicham Achebak, Ana M Vicedo-Cabrera, Sonia I Seneviratne, and Joan Ballester. Mortality burden attributed to anthropogenic warming during Europe's 2022 record-breaking summer. *npj Climate and Atmospheric Science*, 7(1):245, 2024.

[35] Jared T Trok, Elizabeth A Barnes, Frances V Davenport, and Noah S Diffenbaugh. Machine learning–based extreme event attribution. *Science Advances*, 10(34):eadl3242, 2024.

[36] Daniel Mitchell, Clare Heaviside, Sotiris Vardoulakis, Chris Huntingford, Giacomo Masato, Benoit P Guillod, Peter Frumhoff, Andy Bowery, David Wallom, and Myles Allen. Attributing

human mortality during extreme heat waves to anthropogenic climate change. *Environmental Research Letters*, 11(7):074006, 2016.

[37] Peter A Stott, Daithi A Stone, and Myles R Allen. Human contribution to the European heatwave of 2003. *Nature*, 432(7017):610–614, 2004.

[38] Emily Black, Mike Blackburn, Giles Harrison, Brian Hoskins, John Methven, et al. Factors contributing to the summer 2003 European heatwave. *Weather*, 59(8):217–223, 2004.

[39] C3S. The year 2024 set to end up as the warmest on record. *Copernicus Monthly Climate Bulletin*, 2024.

[40] Noah S Diffenbaugh and Elizabeth A Barnes. Data-driven predictions of peak warming under rapid decarbonization. *Geophysical Research Letters*, 51(23):e2024GL111832, 2024.

[41] Kai Chen, Evan De Schrijver, Sidharth Sivaraj, Francesco Sera, Noah Scovronick, Leiwen Jiang, Dominic Roye, Eric Lavigne, Jan Kyselỳ, Aleš Urban, et al. Impact of population aging on future temperature-related mortality at different global warming levels. *Nature communications*, 15(1):1796, 2024.

[42] Eurostat. Population projections in the EU. Technical report, European Commission, 2023.

[43] Christopher W Callahan, Jared Trok, Andrew Wilson, Carlos Gould, Sam Heft-Neal, Marshall Burke, and Noah S Diffenbaugh. Revisiting the contribution of climate change to mortality during the 2003 European heat wave. *in preparation*, 2025.

[44] Martin-Immanuel Bittner, Eva Franziska Matthies, Dafina Dalbokova, and Bettina Menne. Are european countries prepared for the next big heat-wave? *The European Journal of Public Health*, 24(4):615–619, 2014.

[45] Richard C Keller. *Fatal isolation: The devastating Paris heat wave of 2003*. University of Chicago Press, 2015.

[46] Marshall Burke, Mustafa Zahid, Mariana CM Martins, Christopher W Callahan, Richard Lee, Tumenkhusel Avirmed, Sam Heft-Neal, Mathew Kiang, Solomon M Hsiang, and David Lobell. Are we adapting to climate change? *National Bureau of Economic Research Working Paper*, 2024.

[47] Richard C Cornes, Gerard van der Schrier, Else JM van den Besselaar, and Philip D Jones. An ensemble version of the e-obs temperature and precipitation data sets. *Journal of Geophysical Research: Atmospheres*, 123(17):9391–9409, 2018.

[48] C3S. ERA5: Fifth generation of ECMWF atmospheric reanalysis of the global climate. *Copernicus Climate Change Service Climate Data Store*, 2017.

[49] D. Chen, M. Rojas, B.H. Samset, K. Cobb, A. Diongue Niang, P. Edwards, S. Emori, S.H. Faria, E. Hawkins, P. Hope, P. Huybrechts, M. Meinshausen, S.K. Mustafa, G.-K. Plattner, and A.-M. Tréguier. Framing, context, and methods. In V. Masson-Delmotte, P. Zhai, A. Pirani, S. L. Connors, C. Péan, S. Berger, N. Caud, Y. Chen, L. Goldfarb, M. I. Gomis, M. Huang, K. Leitzell, E. Lonnoy, J. B. R. Matthews, T. K. Maycock, T. Waterfield, O. Yelekçi, R. Yu, and B. Zhou, editors, *Climate Change 2021: The Physical Science Basis. Contribution of Working Group I to the Sixth Assessment Report of the Intergovernmental Panel on Climate Change*, chapter 1, pages 147–286. Cambridge University Press, Cambridge, UK and New York, NY, USA, 2021. doi: 10.1017/9781009157896.003.

[50] Olivier Deschenes and Enrico Moretti. Extreme weather events, mortality, and migration. *The Review of Economics and Statistics*, 91(4):659–681, 2009.

[51] Alan Barreca, Karen Clay, Olivier Deschenes, Michael Greenstone, and Joseph S Shapiro. Adapting to climate change: The remarkable decline in the US temperature-mortality relationship over the twentieth century. *Journal of Political Economy*, 124(1):105–159, 2016.

[52] Marshall Burke, Felipe González, Patrick Baylis, Sam Heft-Neal, Ceren Baysan, Sanjay Basu, and Solomon Hsiang. Higher temperatures increase suicide rates in the united states and mexico. *Nature climate change*, 8(8):723–729, 2018.

[53] Tamma A Carleton and Solomon M Hsiang. Social and economic impacts of climate. *Science*, 353(6304):aad9837, 2016.

[54] Tamma A Carleton. Crop-damaging temperatures increase suicide rates in India. *Proceedings of the National Academy of Sciences*, 114(33):8746–8751, 2017.

[55] Garth Heutel, Nolan H Miller, and David Molitor. Adaptation and the mortality effects of temperature across us climate regions. *The Review of Economics and Statistics*, 103(4):740–753, 2021.

[56] Solomon Hsiang. Climate econometrics. *Annual Review of Resource Economics*, 8:43–75, 2016.

[57] Antonio Gasparrini, Yuming Guo, Masahiro Hashizume, Eric Lavigne, Antonella Zanobetti, Joel Schwartz, Aurelio Tobias, Shilu Tong, Joacim Rocklöv, Bertil Forsberg, et al. Mortality risk attributable to high and low ambient temperature: a multicountry observational study. *The Lancet*, 386(9991):369–375, 2015.

[58] Ana Maria Vicedo-Cabrera, N Scovronick, Francesco Sera, Dominic Royé, Rochelle Schneider, Aurelio Tobias, Christofer Astrom, Y Guo, Y Honda, DM Hondula, et al. The burden of heat-related mortality attributable to recent human-induced climate change. *Nature Climate Change*, 11(6):492–500, 2021.

[59] J. Y. Lee, J. Marotzke, G. Bala, L. Cao, S. Corti, J. P. Dunne, F. Engelbrecht, E. Fischer, J. C. Fyfe, C. Jones, A. Maycock, J. Mutemi, O. Ndiaye, S. Panickal, and T. Zhou. Future global climate: Scenario-based projections and near-term information. In V. Masson-Delmotte, P. Zhai, A. Pirani, S. L. Connors, C. Péan, S. Berger, N. Caud, Y. Chen, L. Goldfarb, M. I. Gomis, M. Huang, K. Leitzell, E. Lonnoy, J. B. R. Matthews, T. K. Maycock, T. Waterfield, O. Yelekçi, R. Yu, and B. Zhou, editors, *Climate Change 2021: The Physical Science Basis. Contribution of Working Group I to the Sixth Assessment Report of the Intergovernmental Panel on Climate Change*, chapter 4. Cambridge University Press, Cambridge, United Kingdom and New York, NY, USA, 2021.

[60] Veronika Eyring, Sandrine Bony, Gerald A Meehl, Catherine A Senior, Bjorn Stevens, Ronald J Stouffer, and Karl E Taylor. Overview of the Coupled Model Intercomparison Project Phase 6 (CMIP6) experimental design and organization. *Geoscientific Model Development*, 9(5):1937–1958, 2016.

[61] Brian C O'Neill, Claudia Tebaldi, Detlef P van Vuuren, Veronika Eyring, Pierre Friedlingstein, George Hurtt, Reto Knutti, Elmar Kriegler, Jean-Francois Lamarque, Jason Lowe, et al. The Scenario Model Intercomparison Project (ScenarioMIP) for CMIP6. *Geoscientific Model Development*, 9(9):3461–3482, 2016.